Mon. Not. R. Astron. Soc. **000**, 1–16 (2009) Printed 21 December 2009 (MN LATEX style file v2.2)

Polarization in young open cluster NGC 6823

Biman J. Medhi [1⋆], Maheswar. G[1], J. C. Pandey[1], Motohide Tamura[2] and R. Sagar[1]
[1] *Aryabhatta Research Institute of Observational Sciences (ARIES), Manora Peak, Nainital - 263 129, India*
[2] *National Astronomical Observatory of Japan, Mitaka, Tokyo 181-8588, Japan*

ABSTRACT
We present multiwavelength linear polarimetric observations of 104 stars towards the region of young open cluster NGC 6823. The polarization towards NGC 6823 is dominated by foreground dust grains and we found the evidence for the presence of several layers of dust towards the line of sight. The first layer of dust is located approximately within 200 pc towards the cluster, which is much closer to the Sun than the cluster ($\sim$ 2.1 kpc). The radial distribution of the position angles for the member stars are found to show a systematic change while the polarization found to reduce towards the outer parts of the cluster and the average position angle of coronal region of the cluster is very close to the inclination of the Galactic parallel ($\sim 32^{\circ}$). The size distribution of the grains within NGC 6823 is similar to those in general interstellar medium. The patchy distribution of foreground dust grains are suggested to be mainly responsible for the both differential reddening and polarization towards NGC 6823. The majority of the observed stars do not show the evidence of intrinsic polarization in their light.

Key words: polarization - dust, extinction - open clusters and associations: individual: NGC 6823

1 INTRODUCTION

The polarization of starlight through selective extinction by aligned/partially aligned and asymmetric dust grains, present in general interstellar medium can be consider as a valuable tool to study both the grain properties like size and shape, and small/large scale structure of interstellar magnetic fields in different line of sight. Although the identity of the dominant grain alignment mechanism has proved to be an intriguing problem in grain dynamics (Lazarian, Goodman & Myers 1997), it is generally believed that the asymmetric grains tend to become aligned to the local magnetic field with their shortest axis parallel to the field. For this orientation, the observed polarization vector is parallel to the plane-of-sky projection of a line-of-sight-averaged magnetic field (Davis & Greenstein 1951). Interstellar polarization strongly varies with wavelength (Serkowski, Mathewson & Ford 1975; Wilking , Lebofsky & Rieke 1982). In particular, the wavelength of maximum interstellar polarization (λ_{max}) is thought to be related to the total-to-selective extinction (R_V) as $R_V = (5.6 \pm 0.3)\lambda_{max}$(Whittet & van Breda 1978). Generally, the unreddened stars show no polarization, if it is not a source of intrinsic polarization. The stars with large colour excess (E(B-V)) the values of polarization P show a wide distribution given by $P/E(B-V)_{max} = 0.090\ mag^{-1}$, where P is measured at visual wavelength (Spitzer 1978).

The polarimetric study of young open clusters can provide us valuable information about the foreground interstellar dust because of the available knowledge on their physical parameters like distance, membership probability (Mp) and colour excess. As a part of an observational programme to carry out the polarimetric observations of young open clusters to investigate the properties like magnetic field orientation, λ_{max} , maximum polarization (P_{max}), etc., (Medhi *et al.* 2007, 2008) we observed the young open cluster NGC 6823, which is Hubble Space Telescope's (HST) polarimetric calibration object (Turnshek *et al.* , 1990). The young open cluster NGC 6823 ($R.A.(J2000) : 19^h43^m09^s, Dec(J2000) : +23^{\circ}18^m00^s; l = 59.402, b = -0.144$) is the central cluster of the Vul OBI association (Morgan *et al.* , 1953). It is located in the local arm (Orion) of our Galaxy. A distance modulus of 11.6 ± 0.01 mag which corresponds to a distance of 2.1 ± 0.1 kpc is estimated for the cluster (Guetter 1992). The bright main sequence stars in NGC 6823 reveal an age of $\sim$ 5 Myr for the cluster, whereas the pre main sequence stars indicate an age of younger than 0.3 Myr (Sagar & Joshi 1981).

To study the interstellar polarization in different direction of our galaxy Hiltner (1956), Hall (1958) and Serkowski (1965) made the polarimetric measurements of few bright stars in the direction of NGC 6823. The four bright stars observed by Hiltner (1956) and Hall (1958), using Corning 3385 (equivalent to V filter) and without (clear) filter respectively, are common and belongs to O and B spectral type.

⋆ E-mail: biman@aries.res.in

Serkowski (1965) had observed 21 stars in V filter and 17 stars in B filter including 3 bright stars observed by Hiltner (1956) and Hall (1958). However they made the observations in survey mode, therefore no firm conclusion could be drawn from their study.

In this paper, we present the results of polarimetric measurements made for 104 stars in B, V and R_C photometric band toward NGC 6823 (brighter than $V \simeq 17$ mag). Out of the 104 stars observed, 42 of them have high membership probability ($M_P \geqslant 0.5$). The paper is organized as following: in section 2 we present observation and data reduction; the results and discussion are presented in section 3 and in section 4 we conclude with a summary.

2 OBSERVATION AND DATA REDUCTION

The polarimetric data for the four fields (centered at *R.A.* : $19^h43^m10^s$, *Dec* : $+23^\circ17^m55^s$; *R.A.* : $19^h43^m24^s$, *Dec* : $+23^\circ12^m26^s$; *R.A.* : $19^h43^m24^s$, *Dec* : $+23^\circ23^m55^s$ and *R.A.* : $19^h42^m4^s$, *Dec* : $+23^\circ17^m43^s$) in NGC 6823 were acquired using ARIES Imaging Polarimeter (AIMPOL; Medhi *et al.* 2007) mounted on the Cassegrain focus of the 104-cm Sampurnanand Telescope of ARIES, Nainital in B, V and R_c photometric bands, on 24^{th} May, 25^{th} May, 06^{th} June and 07^{th} June 2007. The imaging was done by using a TK 1024×1024 pixel^2 CCD camera. Each pixel of the CCD corresponds to 1.7 arcsec and the field of view is ~ 8 arcmin diameter on the sky. The FWHM of the stellar image varies from 2 to 3 *pixel*. The read out noise and gain of the CCD are 7.0 e^- and 11.98 e^-/ADU, respectively. The fluxes for all of our programme stars were extracted by aperture photometry after the bias subtraction in the standard manner using IRAF. Instead of robust flat fielding technique we used equation (3) to make uniform response, as mentioned below.

AIMPOL consists of a half wave plate and a Wollaston prism analyzer placed in the telescope beam path to produce ordinary and extraordinary images in slightly different directions separated by ~ 27 *pixels*. To re-image the telescope focal plane on the surface of CCD a focal reducer (85mm, f/1.8) is placed between Wollaston prism and CCD camera with a reduction factor of about 4.7.

By definition, the ratio R(α) is given by,

$$R(\alpha) = \frac{I_e/I_\circ - 1}{I_e/I_\circ + 1} = P\ cos(2\theta - 4\alpha) \quad (1)$$

which is the difference between the intensities of the ordinary ($I_\circ$) and extraordinary (I_e) beams to their sum, P is the fraction of the total light in the linearly polarized condition and θ is the position angle of plane of polarization. It is denoted by normalized Stokes' parameter q (=Q/I), when the half wave plate's fast axis is aligned to the reference axis ($\alpha = 0^\circ$). Similarly, the normalized Stokes' parameter $u\ (= U/I), q_1\ (= Q_1/I), u_1\ (= U_1/I)$ are also the ratios R(α), when the half wave plate are at 22.5°, 45° and 67.5° respectively. In principle, P and θ can be determined by using only two Stokes' parameters q and u. In reality, the situation is not so simple because of two reasons (i) the responsivity of the system to the two orthogonal polarization components may not be same and (ii) the responsivity of the CCD is a function of position on its surface. So, the signals which are actually measured in the two images ($I'_\circ$ *and* I'_e) may differ from the observed one by the following formula (Ramaprakash 1998)

$$\frac{I_e(\alpha)}{I_\circ(\alpha)} = \frac{I'_e(\alpha)}{I'_\circ(\alpha)} \times \frac{F_\circ}{F_e} \quad (2)$$

and the Eq.(1) can be rewrite as

$$R(\alpha) = \frac{(I'_e/I'_\circ \times F_\circ/F_e) - 1}{(I'_e/I'_\circ \times F_\circ/F_e) + 1} = P\ cos(2\theta - 4\alpha) \quad (3)$$

where $F_\circ$ and F_e represent the effects mentioned above and the ratio is given by,

$$\frac{F_\circ}{F_e} = \left[\frac{I'_\circ(0^\circ)}{I'_e(45^\circ)} \times \frac{I'_\circ(45^\circ)}{I'_e(0^\circ)} \times \frac{I'_\circ(22.5^\circ)}{I'_e(67.5^\circ)} \times \frac{I'_\circ(67.5^\circ)}{I'_e(22.5^\circ)}\right]^{1/4} \quad (4)$$

Substituting the ratio in equation (3) and fitting the cosine curve to the four values of $R(\alpha)$, the values of P and θ could be obtained. The individual errors associated with the four values of $R(\alpha)$ putting as a weight while calculating P, θ and their respective errors.

Four polarimetric standard stars and four secondary polarimetric standard stars for null polarization and for the zero point of the polarization position angle were taken from Schmidt, Elston & Lupie (1992) and Turnshek *et al.* (1990) respectively. The observed degree of polarization in percentage ($P\%$) and position angle in degree (θ°) for the polarized standard stars and their corresponding values from Schmidt, Elston & Lupie (1992), Turnshek *et al.* (1990) are given in Table 1. The observed values of $P\%$ and θ° are in good agreement with those given in Schmidt, Elston & Lupie (1992) and Turnshek *et al.* (1990) within the observational errors. The observed normalized stokes parameters q and u in percentage ($q\%, u\%$) for standard unpolarized stars are also given in Table 1. The average value of instrumental polarization is found to be less than 0.05% in all pass-bands. The instrumental polarization of AIMPOL on the 104-cm Sampurnanand Telescope has been monitored since 2004 in different projects and found nearly invariable in different pass-bands (Rautela, Joshi & Pandey 2004; Medhi *et al.* 2007, 2008; Pandey *et al.* 2009)

AIMPOL have no grid, placed to avoid the overlapping of ordinary image of one source with the extraordinary of an adjacent one located 27 *pixels* away along the north-south direction. So, we avoided the central crowded portion of the cluster. However, the fields are chosen in such a manner to include maximum number of member stars. We also had a large number of sources which are not members but are present in the fields observed. All the sources were manually checked and rejected in case of an overlapping image.

3 RESULTS AND DISCUSSION

The results of our polarimetric observations towards NGC 6823 are presented in the Table 2 and Table 3. Star's identification numbers ID(M) and ID(B) are given in column 1 and 2 following this observation and Barkhatova (1957) respectively. The instrumental magnitudes obtained in V filter are given in column 3. The measured values of polarization $P\%$ and their corresponding error $\epsilon\%$ in B, V and R_c filters are given in columns 4, 6 and 8, respectively. The polarization position angle (of the E vector) θ° and the corresponding error ϵ° in B, V and R_c filters are given in columns 5, 7 and

Table 1. Observed polarized and unpolarized standard stars

	Polarized Standard				Unpolarized Standard	
Filter	$P \pm \epsilon(\%)$	$\theta \pm \epsilon(^\circ)$	$P \pm \epsilon(\%)$	$\theta \pm \epsilon(^\circ)$	$q(\%)$	$u(\%)$
	Schmidt, Elston & Lupie(1992)		This work		This work	
		Hiltner-960			HD21447	
B	5.72 ± 0.06	55.06 ± 0.31	5.69 ± 0.20	55 ± 2	0.019	0.011
V	5.66 ± 0.02	54.79 ± 0.11	5.61 ± 0.14	53 ± 2	0.037	- 0.031
R	5.21 ± 0.03	54.54 ± 0.16	5.20 ± 0.06	54 ± 2	- 0.035	- 0.039
		HD 204827			HD12021	
B	5.65 ± 0.02	58.20 ± 0.11	5.72 ± 0.09	59 ± 2	- 0.081	0.071
V	5.32 ± 0.02	58.73 ± 0.08	5.35 ± 0.03	60 ± 2	0.042	- 0.045
R	4.89 ± 0.03	59.10 ± 0.17	4.90 ± 0.20	59 ± 2	0.020	0.031
		BD+64°106			HD14069	
B	5.51 ± 0.09	97.15 ± 0.47	5.46 ± 0.10	99 ± 2	0.038	- 0.010
V	5.69 ± 0.04	96.63 ± 0.18	5.58 ± 0.11	97 ± 2	0.021	0.018
R	5.15 ± 0.10	96.74 ± 0.54	5.20 ± 0.02	97 ± 2	0.010	- 0.014
		HD 19820			G191B2B	
B	4.70 ± 0.04	115.70 ± 0.22	4.75 ± 0.20	114 ± 2	0.072	- 0.059
V	4.79 ± 0.03	114.93 ± 0.17	4.81 ± 0.10	114 ± 2	- 0.022	- 0.041
R	4.53 ± 0.03	114.46 ± 0.17	4.65 ± 0.13	113 ± 2	- 0.036	0.027

Secondary Polarized Standard					
Star Name	Filter	$P \pm \epsilon(\%)$	θ	$P \pm \epsilon(\%)$	$\theta \pm \epsilon(^\circ)$
		Turnshek *et al.* (1990)		This work	
NGC6823-2j	V	2.67 ± 0.11	13.0	2.70 ± 0.01	11 ± 2
NGC6823-6j	V	3.23 ± 0.13	09.0	3.24 ± 0.07	08 ± 2
NGC6823-7j	V	3.74 ± 0.13	06.9	3.74 ± 0.15	06 ± 2
NGC6823-10j	V	4.55 ± 0.13	07.2	4.57 ± 0.01	06 ± 2

Table 4. Results of previous polarization measurements carried out by Serkowski (1965) in the direction of NGC 6823.

ID(B) (1)	$P_B \pm \epsilon(\%)$ (2)	θ_B (3)	$P_V \pm \epsilon(\%)$ (4)	θ_V (5)	M_P (6)
	Serkowski (1965)				
3	4.14 ± 0.23	06	4.19 ± 0.23	06	0.97
9	4.51 ± 0.32	172	4.84 ± 0.32	175	0.97
11	5.11 ± 0.46	05	4.47 ± 0.46	04	0.97
13	2.95 ± 0.14	11	3.32 ± 0.14	09	0.95
17	2.81 ± 0.51	13	3.36 ± 0.51	16	0.97
54	—	—	0.83 ± 0.28	03	—
68	4.38 ± 0.46	14	5.34 ± 0.46	12	0.96
73	—	—	0.23 ± 0.18	30	—
74	2.58 ± 0.46	13	3.64 ± 0.46	12	0.97
78	3.41 ± 0.55	02	4.10 ± 0.55	09	0.93
189	—	—	0.23 ± 0.14	52	—
$BD + 23°3745$	6.40 ± 0.14	27	6.63 ± 0.14	24	0.88

9, respectively. The position angles in the equatorial coordinate system are measured from the north increasing eastward. Columns 10 and 11 represent the membership probabilities $M_P(E)$ and $M_P(D)$ according to Erickson (1971) and Dias *et al.* (2006), respectively. Stars with $M_P \geqslant 0.50$ are considered as cluster members in this study.

The previous polarimetric measurements of stars in the direction of NGC 6823 carried out by Serkowski (1965) is presented in Table 4. Serkowski (1965) observed 22 stars in the direction of NGC 6823 using B and V photometric bands. Out of 22 stars observed by Serkowski (1965) we have included only 12 stars in our study which have the available R.A. and Dec. In column 1, we give the identification numbers which are adopted from Barkhatova (1957). $P\%$ and θ° in B and V filters are given in columns 2, 3, 4 and 5, respectively. We converted p to P per cent using the relation P per cent$= 46.05p$ (Whittet 1992). In column 6 we give the membership probabilities of stars obtained from Erickson (1971).

Figure 2 presents the sky projection of the V-band polarization vectors for the 104 stars observed by us in NGC 6823 (R band image is reproduced from Digitized Sky Survey II). The polarization vectors are drawn at the center of the observed stars. The length of the polarization vector is proportional to the percentage of polarization in V band (P_V) and it is oriented parallel to the direction of corresponding observed polarization position angle in degree in V band (θ_V). The dashed line represents the Galactic parallel at $b = -0.14^\circ$ inclined at $\sim 32^\circ$ with respect to the north. The stars with $M_P \geqslant 0.50$ are identified using closed star symbols in white colour. Polarization vectors for 12 stars observed by Serkowski (1965) are shown in white colour.

In Figure 3, we present the sky projection of the B-band polarization vectors for the 104 stars observed by us towards NGC 6823 (vectors in black colour) along with the results from Serkowski (1965) (vectors in white colour) and in Figure 4 we present only the sky projection of the R_c-band polarization vectors for the 104 stars observed by us

Table 2. Observed B, V and R_c polarization values for different stars in NGC 6823

ID(M)† (1)	ID(B)†† (2)	V(mag) (3)	$P_B \pm \epsilon$ (%) (4)	$\theta_B \pm \epsilon$ (°) (5)	$P_V \pm \epsilon$ (%) (6)	$\theta_V \pm \epsilon$ (°) (7)	$P_R \pm \epsilon$ (%) (8)	$\theta_R \pm \epsilon$ (°) (9)	$M_p(E)$* (10)	$M_p(D)$** (11)
01	—	16.06	1.93 ±0.54	26 ±9	2.15 ±0.32	32 ±5	1.88 ±0.17	25 ±4	—	—
02	20	14.98	4.13 ±0.16	2 ±2	4.39 ±0.09	2 ±2	4.28 ±0.11	4 ±2	0.96	0.86
03	74	13.77	2.56 ±0.05	9 ±2	2.70 ±0.01	11 ±2	2.55 ±0.03	9 ±2	0.97	0.72
04	73	11.47	0.50 ±0.07	23 ±8	0.52 ±0.09	25 ±5	0.51 ±0.01	22 ±3	—	—
05	18	16.36	3.47 ±0.18	9 ±2	3.34 ±0.55	12 ±5	3.54 ±0.23	5 ±2	—	0.00
06	23	16.29	2.32 ±0.70	22 ±5	2.51 ±0.14	22 ±2	2.47 ±0.07	26 ±2	—	0.88
07	17	14.2	3.72 ±0.01	4 ±2	3.74 ±0.15	6 ±2	3.73 ±0.03	5 ±2	0.97	0.77
08	78	14.27	3.15 ±0.03	2 ±2	3.69 ±0.07	4 ±2	3.44 ±0.08	2 ±2	0.93	0.80
09	—	16.25	4.17 ±0.21	4 ±2	4.10 ±0.30	5 ±2	4.12 ±0.08	3 ±2	—	0.83
10	27	15.05	1.97 ±0.01	23 ±2	2.18 ±0.14	27 ±2	2.11 ±0.15	22 ±3	—	0.01
11	26	13.86	1.99 ±0.07	18 ±2	1.98 ±0.06	20 ±2	1.88 ±0.03	16 ±2	—	0.00
12	13	11.98	3.06 ±0.09	8 ±2	3.13 ±0.06	12 ±2	3.06 ±0.04	8 ±2	0.95	0.81
13	28	16.4	3.42 ±0.52	3 ±4	3.78 ±0.49	5 ±4	3.79 ±0.04	8 ±2	—	0.88
14	75	15.19	2.13 ±0.16	23 ±2	2.15 ±0.17	23 ±3	2.20 ±0.05	24 ±2	—	0.88
15	77	15.13	1.63 ±0.03	21 ±2	1.72 ±0.03	27 ±2	1.66 ±0.29	33 ±6	—	0.45
16	76	15.78	3.12 ±0.15	5 ±2	3.24 ±0.07	8 ±2	3.19 ±0.01	5 ±2	—	0.84
17	16	16.06	3.15 ±0.11	3 ±2	3.73 ±0.31	5 ±2	3.08 ±0.28	4 ±3	—	—
18	71	15.67	0.98 ±0.18	26 ±7	1.24 ±0.10	17 ±3	1.01 ±0.08	17 ±3	—	0.34
19	70	16.49	4.01 ±0.29	3 ±2	4.09 ±0.16	4 ±2	3.85 ±0.41	7 ±3	—	0.89
20	68	13.93	4.50 ±0.06	4 ±2	4.57 ±0.01	6 ±2	4.48 ±0.20	4 ±2	0.96	0.81
21	12	16.26	0.62 ±0.03	168 ±3	0.80 ±0.17	174 ±4	0.66 ±0.13	179 ±3	—	0.00
22	11	13.54	5.04 ±0.08	3 ±2	5.28 ±0.05	4 ±2	4.94 ±0.03	2 ±2	0.97	0.82
23	4	13.63	0.52 ±0.05	23 ±9	0.55 ±0.04	23 ±9	0.53 ±0.05	24 ±8	—	0.00
24	9	13.79	4.46 ±0.04	12 ±2	4.40 ±0.03	13 ±2	4.22 ±0.13	12 ±2	0.97	0.77
25	8	15.82	1.79 ±0.19	29 ±3	1.83 ±0.06	19 ±2	1.81 ±0.09	26 ±2	—	0.82
26	5	14.88	1.49 ±0.20	26 ±4	1.82 ±0.15	35 ±3	1.41 ±0.21	40 ±6	—	0.72
27	64a	14.5	3.33 ±0.37	96 ±3	3.39 ±0.32	98 ±3	3.25 ±0.07	94 ±2	—	0.00
28	65	15.56	5.21 ±0.51	7 ±3	5.07 ±0.17	4 ±2	4.97 ±0.10	2 ±2	—	0.76
29	64	15.07	0.86 ±0.23	21 ±8	0.83 ±0.10	18 ±7	0.80 ±0.05	20 ±4	—	0.00
30	62	14.63	1.34 ±0.24	26 ±6	1.44 ±0.27	28 ±7	1.39 ±0.31	23 ±8	0.95	0.82
31	61	15.49	0.95 ±0.13	27 ±7	0.94 ±0.16	21 ±4	0.91 ±0.18	21 ±7	—	0.41
32	63	16.31	1.40 ±0.22	15 ±6	1.42 ±0.23	20 ±9	1.44 ±0.29	24 ±8	—	0.59
33	65a	16.09	1.19 ±0.24	17 ±7	1.22 ±0.28	17 ±9	1.27 ±0.22	16 ±7	—	0.77
34	—	16.51	0.94 ±0.18	35 ±7	1.23 ±0.21	42 ±7	0.99 ±0.17	32 ±8	—	0.87
35	25	16.48	3.68 ±0.22	2 ±3	3.73 ±0.11	6 ±2	3.99 ±0.26	4 ±6	—	0.89
36	—	16.44	3.03 ±0.25	8 ±2	3.03 ±0.39	7 ±4	2.83 ±0.31	4 ±3	—	—
37	10	16.44	5.94 ±0.18	9 ±2	5.50 ±0.93	9 ±6	5.55 ±0.18	12 ±2	—	0.48
38	—	16.71	3.47 ±0.23	12 ±2	3.71 ±0.65	16 ±5	3.41 ±0.22	18 ±2	—	0.45
39	—	16.43	4.88 ±0.09	15 ±2	4.92 ±0.15	13 ±2	4.83 ±0.06	12 ±2	—	0.89
40	14	14.17	2.88 ±0.06	2 ±2	3.31 ±0.05	3 ±2	2.97 ±0.06	3 ±2	0.97	0.85
41	33	14.99	0.99 ±0.14	16 ±9	1.06 ±0.18	18 ±8	1.01 ±0.13	11 ±5	0.82	0.83
42	36	15.71	2.26 ±0.21	25 ±4	2.42 ±0.23	31 ±3	2.35 ±0.05	27 ±2	—	0.57
43	—	16.77	2.29 ±0.67	30 ±8	2.34 ±0.54	32 ±7	2.27 ±0.42	35 ±5	—	—
44	34	13.91	3.52 ±0.10	9 ±2	3.65 ±0.16	10 ±2	3.55 ±0.03	10 ±2	0.98	0.59
45	51	16.06	1.91 ±0.20	11 ±4	2.10 ±0.11	18 ±2	1.96 ±0.17	16 ±2	—	0.01
46	53	16.09	1.79 ±0.30	15 ±6	1.85 ±0.28	19 ±5	1.76 ±0.06	18 ±2	—	0.02
47	35	11.37	1.52 ±0.02	29 ±2	1.63 ±0.09	29 ±2	1.47 ±0.10	28 ±2	0.79	—
48	50	14.32	0.55 ±0.02	42 ±2	0.62 ±0.08	44 ±9	0.58 ±0.06	38 ±7	—	—
49	49	15.49	1.16 ±0.13	17 ±4	1.09 ±0.06	18 ±2	1.09 ±0.10	11 ±4	—	—
50	—	16.48	1.65 ±0.36	26 ±7	1.76 ±0.36	33 ±7	1.78 ±0.22	35 ±4	—	—
51	42	13.92	0.88 ±0.16	12 ±9	0.98 ±0.01	15 ±2	0.95 ±0.01	13 ±2	—	—
52	98	14.38	1.35 ±0.39	17 ±8	1.44 ±0.31	19 ±5	1.47 ±0.32	17 ±3	—	0.00
53	99	16.01	2.52 ±0.47	24 ±4	2.75 ±0.28	26 ±3	2.46 ±0.14	22 ±4	—	0.00
54	80	14.27	1.75 ±0.07	17 ±2	2.15 ±0.25	20 ±4	1.83 ±0.12	18 ±4	—	0.69
55	79	15.37	3.02 ±0.15	21 ±2	3.20 ±0.64	21 ±2	3.11 ±0.66	27 ±2	—	0.82
56	—	15.57	3.16 ±0.18	10 ±2	3.39 ±0.52	13 ±5	3.26 ±0.33	11 ±2	—	0.02
57	81	14.32	4.02 ±0.21	172 ±2	4.54 ±0.11	176 ±2	3.93 ±0.15	170 ±5	—	—
58	—	16.70	1.96 ±0.37	28 ±9	2.26 ±0.27	29 ±4	2.01 ±0.26	24 ±4	—	0.73
59	82	13.29	0.87 ±0.13	19 ±6	0.91 ±0.08	19 ±5	0.85 ±0.04	18 ±4	0.55	—
60	125	15.01	0.61 ±0.10	24 ±8	0.79 ±0.08	28 ±6	0.68 ±0.04	26 ±5	—	—
61	—	15.43	2.35 ±0.25	16 ±9	2.89 ±0.20	21 ±6	2.65 ±0.22	17 ±2	—	0.29
62	—	12.19	0.59 ±0.04	37 ±4	0.67 ±0.07	38 ±6	0.63 ±0.11	34 ±4	—	—

Table 3. Continuation of Table 2

ID(M)† (1)	ID(B)†† (2)	V(mag) (3)	$P_B \pm \epsilon$ (%) (4)	$\theta_B \pm \epsilon$ (°) (5)	$P_V \pm \epsilon$ (%) (6)	$\theta_V \pm \epsilon$ (°) (7)	$P_R \pm \epsilon$ (%) (8)	$\theta_R \pm \epsilon$ (°) (9)	$M_p(E)$* (10)	$M_p(D)$** (11)
63	96	15.06	1.73 ±0.39	12 ±3	1.68 ±0.33	13 ±4	1.64 ±0.20	10 ±3	—	0.00
64	—	15.82	2.85 ±0.42	6 ±5	3.20 ±0.45	9 ±4	2.79 ±0.14	7 ±5	—	—
65	—	16.29	4.80 ±0.34	41 ±3	4.86 ±0.34	38 ±3	4.77 ±0.32	36 ±4	—	—
66	—	15.08	1.65 ±0.45	8 ±9	1.63 ±0.14	13 ±3	1.55 ±0.23	12 ±3	—	—
67	88	14.12	0.65 ±0.10	6 ±5	0.72 ±0.05	8 ±4	0.66 ±0.04	7 ±4	—	0.40
68	—	15.65	1.35 ±0.20	36 ±3	1.39 ±0.17	37 ±2	1.27 ±0.17	36 ±3	—	0.58
69	86	14.50	0.95 ±0.30	23 ±6	1.21 ±0.18	25 ±6	1.01 ±0.11	24 ±6	—	—
70	127	15.41	3.04 ±0.06	10 ±2	3.42 ±0.06	18 ±2	3.32 ±0.03	11 ±2	—	—
71	130	14.83	1.11 ±0.13	23 ±6	1.21 ±0.07	32 ±2	1.25 ±0.23	28 ±8	—	—
72	129	14.66	3.96 ±0.27	15 ±2	4.20 ±0.36	14 ±2	3.76 ±0.06	17 ±2	—	—
73	95	14.38	1.32 ±0.13	33 ±3	1.45 ±0.08	35 ±2	1.37 ±0.05	31 ±2	0.75	—
74	93	12.08	2.69 ±0.01	6 ±2	2.74 ±0.04	4 ±2	2.52 ±0.09	2 ±2	0.97	0.81
75	94	14.50	2.82 ±0.55	10 ±6	3.16 ±0.44	17 ±4	2.79 ±0.12	9 ±2	—	—
76	91	12.27	3.01 ±0.03	11 ±2	3.23 ±0.08	12 ±2	3.06 ±0.10	13 ±2	0.95	—
77	—	15.33	1.27 ±0.08	166 ±2	1.26 ±0.09	165 ±3	1.18 ±0.14	161 ±5	—	—
78	—	15.78	1.50 ±0.29	22 ±3	1.66 ±0.23	24 ±3	1.43 ±0.08	16 ±2	—	—
79	—	16.19	1.96 ±0.19	5 ±3	2.31 ±0.24	10 ±3	2.02 ±0.39	8 ±5	—	—
80	—	16.3	3.23 ±0.22	21 ±2	3.37 ±0.40	24 ±4	3.46 ±0.35	29 ±6	—	0.89
81	128	16.26	4.02 ±0.29	6 ±6	4.12 ±0.28	8 ±5	4.15 ±0.12	9 ±3	—	—
82	—	14.54	0.89 ±0.22	7 ±4	1.01 ±0.20	8 ±3	0.85 ±0.21	4 ±4	—	0.46
83	—	14.35	1.29 ±0.12	21 ±3	1.51 ±0.11	25 ±2	1.15 ±0.19	19 ±3	—	—
84	—	14.29	1.16 ±0.09	12 ±3	1.21 ±0.16	18 ±6	1.07 ±0.14	10 ±5	—	—
85	—	11.78	0.73 ±0.02	24 ±3	0.76 ±0.03	21 ±2	0.77 ±0.05	27 ±3	—	—
86	—	15.99	2.63 ±0.50	110 ±7	2.78 ±0.58	113 ±8	2.79 ±0.62	116 ±8	—	—
87	—	15.44	3.58 ±0.21	20 ±2	3.67 ±0.10	27 ±2	3.48 ±0.06	25 ±2	—	—
88	—	13.86	2.35 ±0.28	30 ±4	2.46 ±0.11	39 ±2	2.34 ±0.12	33 ±2	—	—
89	—	15.64	3.11 ±0.32	12 ±6	3.41 ±0.28	15 ±4	3.26 ±0.43	18 ±8	—	—
90	—	15.81	4.17 ±0.68	30 ±6	4.23 ±0.35	37 ±2	4.26 ±0.12	37 ±2	—	—
91	—	16.21	3.18 ±0.27	21 ±3	3.24 ±0.12	24 ±2	3.16 ±0.48	20 ±5	—	—
92	184	13.82	3.21 ±0.11	24 ±2	3.16 ±0.21	21 ±2	3.17 ±0.28	24 ±2	—	—
93	179	13.12	1.85 ±0.20	17 ±3	2.05 ±0.17	21 ±2	1.87 ±0.05	19 ±2	0.97	0.89
94	180	12.5	2.49 ±0.02	15 ±2	2.75 ±0.17	16 ±2	2.41 ±0.02	16 ±2	—	0.00
95	—	15.05	2.45 ±0.44	27 ±5	2.60 ±0.29	25 ±3	2.35 ±0.20	21 ±3	—	—
96	191	14.3	2.54 ±0.21	19 ±3	2.87 ±0.44	18 ±8	2.48 ±0.27	22 ±3	—	—
97	—	14.38	2.17 ±0.59	18 ±8	2.27 ±0.09	25 ±2	2.27 ±0.39	28 ±5	—	—
98	185	14.48	2.78 ±0.29	18 ±4	2.89 ±0.26	23 ±2	2.69 ±0.31	18 ±3	—	0.88
99	22	14.88	2.20 ±0.43	36 ±6	2.27 ±0.36	38 ±5	2.16 ±0.11	37 ±4	—	0.07
100	186	14.67	3.51 ±0.17	10 ±2	3.77 ±0.03	13 ±2	3.60 ±0.16	13 ±2	—	0.57
101	192	14.96	2.73 ±0.10	35 ±2	3.04 ±0.37	27 ±3	2.55 ±0.23	21 ±3	—	0.47
102	187	14.37	2.97 ±0.05	20 ±2	3.29 ±0.02	18 ±2	2.75 ±0.10	20 ±2	—	0.81
103	—	14.63	4.11 ±0.93	13 ±2	4.20 ±0.46	15 ±3	3.95 ±0.52	15 ±4	—	0.89
104	29	15.33	4.30 ±0.06	11 ±2	4.33 ±0.06	12 ±2	4.35 ±0.25	10 ±2	—	0.24

† : According to this observation
†† : According to Barkhatova (1957)
* : According to Erickson (1971)
** : According to Dias *et al.* (2006)

in NGC 6823 (vectors in black colour), because there is no observations by Serkowski (1965) in R filter.

There are eight stars in common between the Serkowski (1965) and present observations. The polarization and position angles for the eight common stars in B and V filters seems to be consistent within the uncertainty in both the observations. From the sky projection of the polarization vectors for 104 stars observed by us in all the three filters, it is clearly exist that the polarization vectors of the stars distributed about the Galactic plane and less than the Galactic plane (especially those located at the center of the cluster).

Figure 5 shows the distribution of the polarization and position angle in V filter (P_V and θ_V) for the 42 member stars with the radial distance from the cluster center. We have chosen $(R.A.(J2000) : 19^h43^m09^s, Dec(J2000) : +23°18^m00^s$ as the center of the cluster taken from Kharchenko *et al.* 2005, where they use the approximation of maximum surface density of cluster members for locating the cluster centre. The upper and lower left panel of the Fig. 5 show the distribution of position angle and polarization in V filter with the radial distance from the center of the cluster. The position angles are found to show a systematic change while the polarization found to reduce towards the outer parts of the cluster. In both the plots it is noticable that the member stars show preferentially two separate distributions which are shown by the histograms in upper

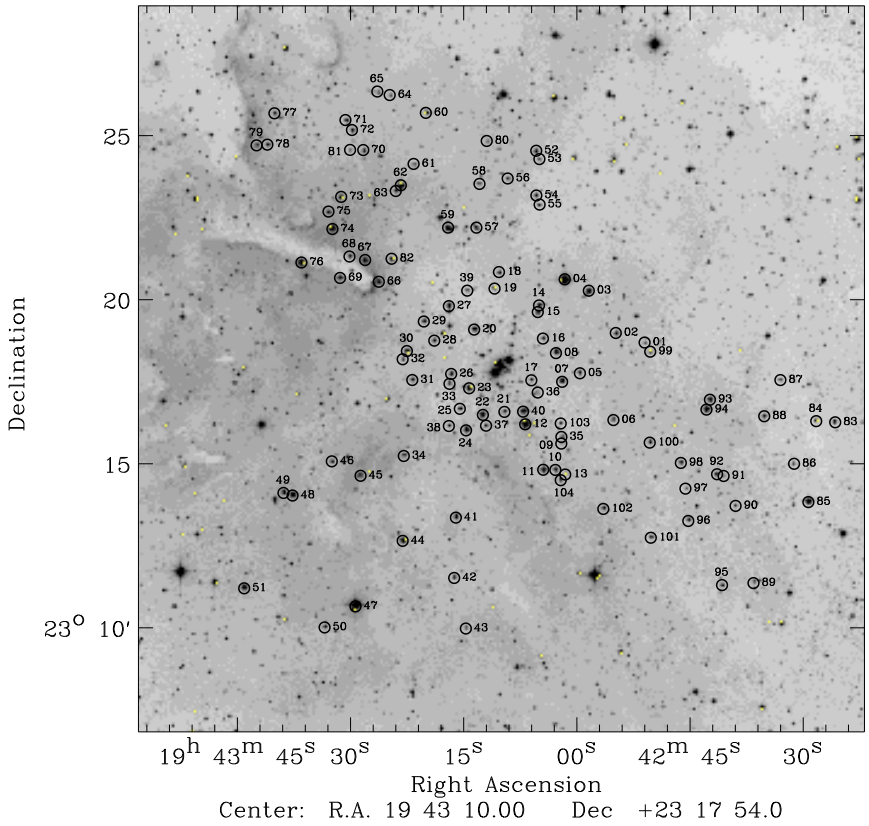

Figure 1. The $25' \times 25'$ R-band DSS2 image of the field containing NGC 6823, reproduced from Digitized Sky Survey II. The field identification is followed by this observation (ID(M)).

and lower right panel of the Fig. 5. From the cluster center to radial distance of 4 arcmin the stars are showing a trend of lower position angle and higher polarization, black filled star symbol than the stars lying at radial distance of above 4 arcmin, black filled circle in the upper and lower left panel of Fig. 5. Stone (1988) also found a boundary at $r \simeq 3.5$ arcmin and he defines the region from cluster center to $r \simeq 3.5$ arcmin as the nucleus and above $r \simeq 3.5$ arcmin as the coronal region of the cluster NGC 6823. Other authors like Barkhatova (1957) found the radius for the nuclear region as $r \simeq 4.0$ arcmin while Turner (1979) quote it as $r \simeq 2.5$ arcmin. In general, every cluster consists of two main regions, a nucleus and a corona. Nucleus is the densest, central part of the cluster, which is perceived directly by our eye as a cluster. Corona is an outer, extended, less dense region around the cluster. For many distant clusters, the coronas are lost against the rich star field.

The right upper and lower panel of the Fig.5 present the distribution of 42 member stars belong to the nucleus and the coronal region shown by the dashed and the filled line histogram. In NGC 6823, out of 42 member stars 24 stars belong to the nucleus and 18 stars belong to the coronal region. Two significantly different distributions of the polarization and the position angle are followed by the stars belong to nucleus and coronal region as shown in the histograms in Fig.5. The weighted mean value of polarization (P_V) and position angle (θ_V) in V filter are 3.66±0.02%, 8°±1 for the nucleus, and 3.10±0.02%, 25°±1 for the coronal region respectively. The average value of the position angle of the coronal region is more closer to the inclination of the Galactic parallel ($\sim 32°$) than the nuclear region. The distribution of polarization vectors about the Galactic plane indicates that the dust grains present in the coronal region are mostly aligned by a magnetic field which is nearly parallel to the direction of the Galactic Disk. Whether in the nucleus the distribution of polarization vectors less than the Galactic plane indicates that a second component of magnetic field which is slightly less inclined to the Galactic Disk could also be present.

In the radial distribution plots (Fig.5), it is also noticed that the polarization (P_V) data points are more scattered in the nucleus as compared to the coronal region while the position angle (θ_V) data points are showing the same behaviour (highly scattered) in both regions. The highly scattered P_V data points in the nuclear region indicate that the density and distributions of the intracluster dust/materials may be higher and more differential respectively than the coronal region. The presence of different generation of dust particles and different component of local magnetic field may be the cause for highly scattered θ_V data points in the radial plot for both regions.

To check the consistency of our results, we use Heiles

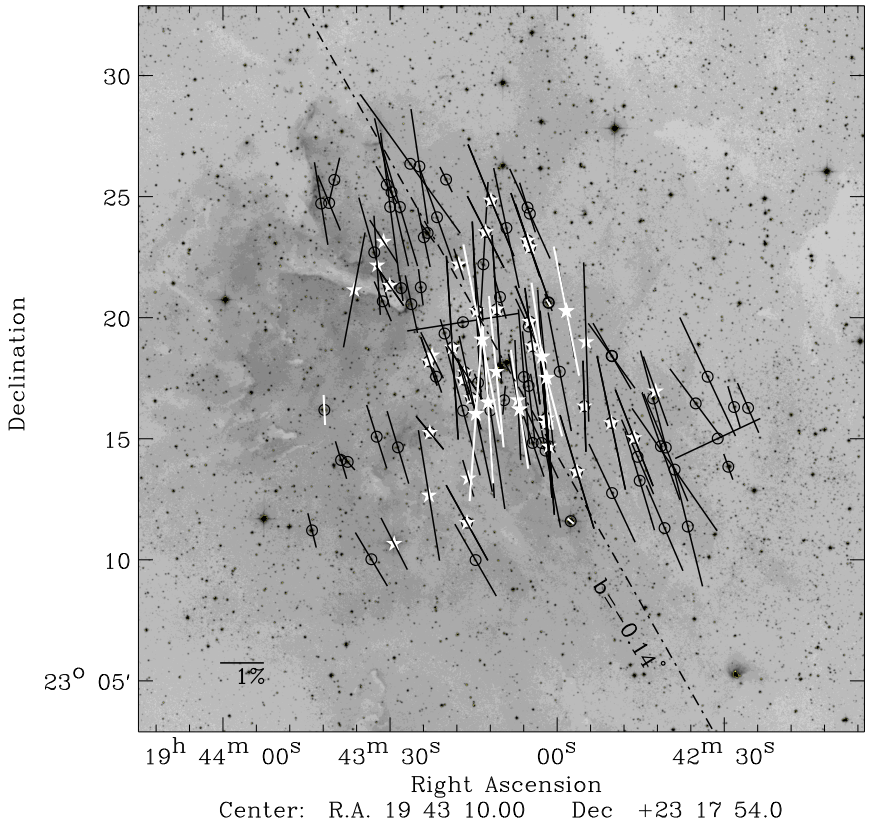

Figure 2. The $30' \times 30'$ R-band DSS2 image of the field containing NGC 6823, reproduced from Digitized Sky Survey II. The position angles, in the equatorial coordinate system, are measured from the north, increasing eastward. The polarization vectors are drawn with the star as the center. Length of the polarization vector is proportional to the percentage of polarization P_V and it is oriented parallel to the direction corresponding to the observed polarization position angle θ_V. A vector with a P of 1% is shown for reference. The dashed line represents the Galactic parallel at $b = -0.14°$. Stars with $M_P \geqslant 0.50$ are identified with closed star symbols in white colour. Polarization vectors of twelve stars observed by Serkowski et al.(1965) are shown in white colour.

(2000) catalogue which has a compilation of over 9000 polarization measurements. We found 19 stars with polarization measurements in V band, within a circular region of radius $\simeq 2°$ around NGC 6823. Figure 6 presents P_V vs. θ_V plot. Our results are represented by open squares. The polarizations and position angles in visual filter taken from Heiles (2000) are represented by filled black circles. The stars with $M_P \geqslant 0.50$ are identified using star symbols. The stars from Heiles (2000) show degree of polarization (P_H) in the ranges from ~ 0.01 to $\sim 6.36\%$. The mean value of P_H and position angle (θ_H) are $\simeq 2.21 \pm 0.86\%$ and $\simeq 28 \pm 10°$, respectively. In our observation, the P_V of the stars are found to be in the ranges from ~ 0.52 to $\sim 5.50\%$. The stars make a clustering towards the lower position angle. The mean value of P_V and θ_V are found to be $\sim 2.58 \pm 0.39\%$ and $\sim 26 \pm 4°$, respectively.

The mean values of polarization and position angles for a smaller region of $\sim 25' \times 25'$ centering at NGC 6823, obtained by us are nearly similar to those for a larger region from Heiles (2000). The cause of polarization is, therefore, must likely be due to the contribution from the dust grains distributed in an extended structure closer to us and from the small intracluster contribution. Consequently, the knowledge about the distribution of interstellar dust towards the direction of NGC 6823 is very important, to interpret the our polarimetric results.

3.1 Distribution of interstellar matter in the region of NGC 6823

The color excess E(B-V) of this cluster for main sequence stars varies from $0^m.60$ to $1^m.16$ (Sagar & Joshi 1981, Sagar 1987). Moreover, a relatively larger value of color excess is found at the center and along the diagonal joining the North-West corner to the South-East corner of the cluster (Sagar & Joshi 1981). In NGC 6823, there is a slight tendency that the E(B-V) for the stars in the eastern part of the cluster exhibit a large value of R_V. The cluster NGC 6823 is surrounded by a reflection nebula NGC 6820. The extinction is highest at the eastern part of the cluster as it is the direction of the reflection nebula. But excluding super-giant the reddening law for the whole cluster can be characterized by $R_V = 3.2 \pm 0.1$ (Guetter 1992).

By using the optical database 'Digitized Sky Survey I' and applying traditional star count technique, Dobashi et al.

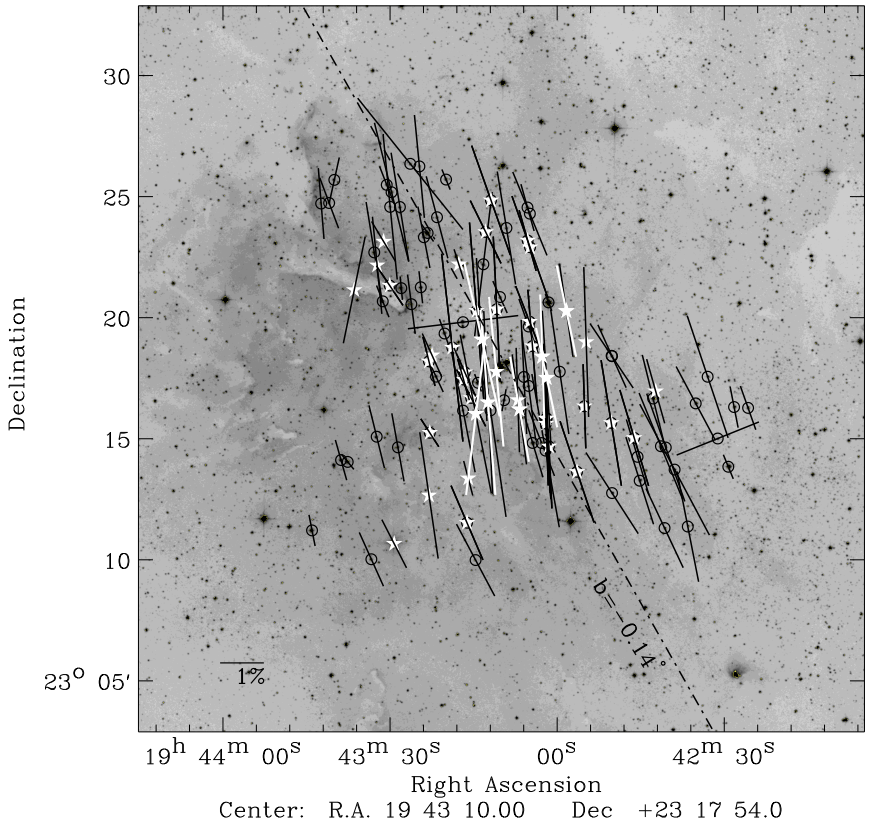

Figure 3. Same as in Figure 2 but for P_B and θ_B. Results for 9 stars observed by Serkowski (1965) using B filter are shown using vectors drawn in white.

(2005) produced extinction maps of the entire region of the Galaxy in the galactic latitude range $|b| \leqslant 40^\circ$. We have used their fits images of the extinction map of the field containing NGC 6823 available on-line [1].

The high resolution extinction map overlaid with V band results from our observations is shown in Figure 7. We transformed all position angles measured relative to the equatorial north to the galactic north using the relation given by Corradi et al. (1998), because the A_V maps are in galactic coordinates. The black circle identifies the center of the cluster ($l = 59.40^\circ$, $b = -0.144^\circ$). The black and white colour-bar on the right hand side of the extinction map shows the range of A_V values in the figure. The contours are plotted at A_V=0.5 to 4 with an interval of 0.5 magnitude.

The extinction towards the location of the cluster (black circle) shows relatively low ($A_V \sim 3$) values. But the outer regions of the cluster especially towards the south and the east, the extinction increases up to $\sim$ 4 magnitude. One clump identified by Dobashi et al.(2005) in this region is labeled as P10 in Figure 7. There is only one dark cloud LDN 791 identified by Lynds (1962) located radially 40′ away from the clump P10 in south east direction. The value of extinction estimated by previous observers (Guetter 1992, Feinstein 1994, Sagar & Joshi 1981) towards the center of the cluster is nearly agree with Dobashi et al.(2005).

The Columbia 1.2-m millimeter-wave telescope CO emission survey in NGC 6823 by Leisawitz, Bash & Thaddeus (1989) identify five molecular clouds around it at the cluster distance. The velocity and masses of the clouds ranges from 23.7 kms^{-1} to 34.8 kms^{-1} and $11 \times 10^3 M_\odot$ to $110 \times 10^3 M_\odot$, respectively. The Balloon-borne Large Aperture Sub-millimeter Telescope (BLAST) also detect sixty compact sub-millimeter sources simultaneously at 250, 350 and 500 μm (Chapin *et al.* 2008) towards NGC 6823. Of these sixty compact sub-millimeter sources, forty nine of them are found to be associated with NGC 6823.

To have an idea about the distances to the foreground dust concentration, it is very important to study the distribution of polarization at different distances in that particular line of sight. So, to investigate the polarization properties/distribution of dust grains towards NGC 6823 located at different distances, we selected all the stars from Heiles (2000) within a circle of radius 5° around NGC 6823 with available polarization data (P_H). The parallax measurements for the stars are obtained from the *Hipparcos and Tycho Catalogs* (Perryman *et al.* 1997 and Hϕg *et al.* 1997). Applying 2σ rejection limit criterion to the parallax, we found parallax measurements available only for 45 stars, covering maximum distances up to 800 pc. Stars which

[1] http://darkclouds.u-gakugei.ac.jp/astronomer/astronomer.html

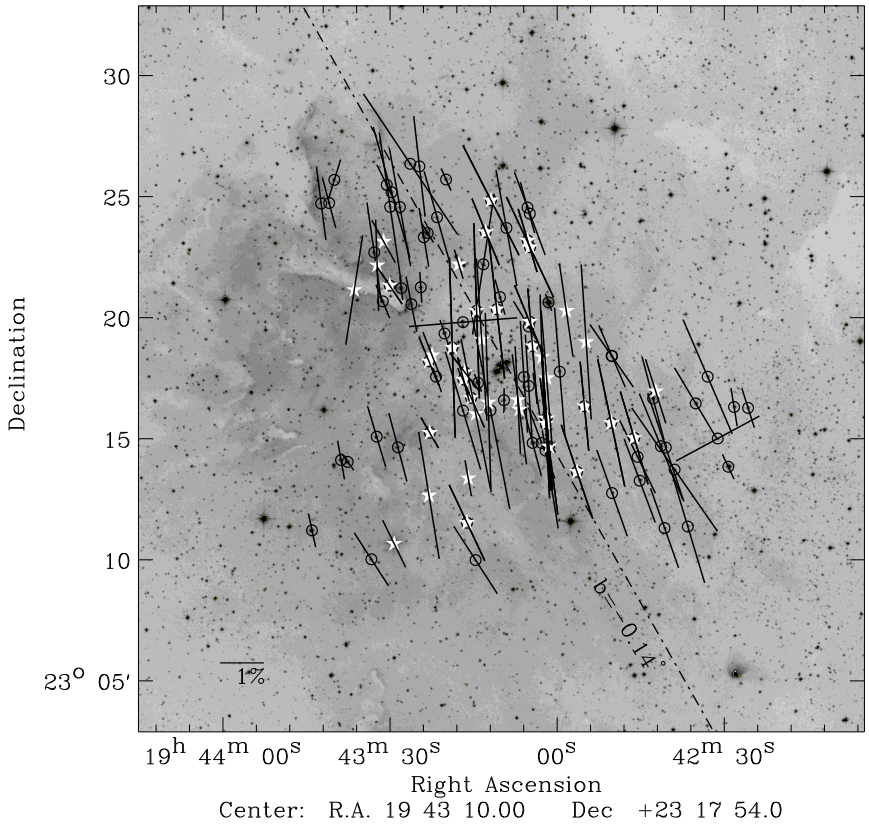

Figure 4. Same as in Figure 2 but for P_R and θ_R.

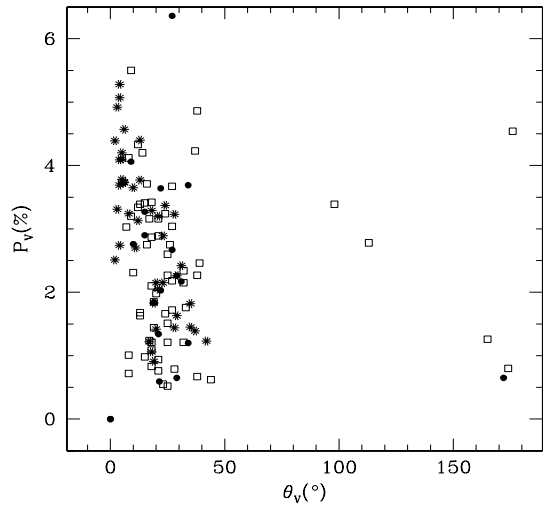

Figure 6. The P_V vs. θ_V plot for 104 stars observed by us in the direction of NGC 6823 are shown using open squares. Stars taken from Heiles (2000) are shown by using filled black circles. The stars with $M_p \geqslant 0.50$ are identified using star symbols.

showed peculiar features and emissions in their spectrum, as given by SIMBAD, are rejected.

Figure 8 presents the degree of polarization (P_H) versus distance plot. The stars located closer to us show low value of P_H ($\lesssim 0.2\%$) than the stars located beyond ~ 200 pc which show relatively high values of P_H in the range from 0.2% to 1.5% with a sharp jump in polarization occurring at ~ 200 pc. Only one star is available in between ~ 10 to ~ 100 pc, so from the Figure 8 we can infer only a maximum distance of 200 pc to the dust grains responsible for the observed sharp jump and assign a maximum distance of 200 pc to the first layer of dust towards NGC 6823.

Since, most of the extinction/reddening is produced by the foreground interstellar material so, it is necessary to investigate about the evolution of the interstellar environments from the Sun to the cluster. In Figure 9, we have plotted the Stokes parameter Q_V ($= P_V cos2\theta_V$) and U_V ($= P_V sin2\theta_V$) in V filter, for each of the 42 observed member stars. In figure, the coordinates Q_V=0 and U_V=0 represent the dustless solar neighbourhood. The points lying at other parts in the figure indicate the direction of the polarization vector as seen from the sun. The member stars over this region roughly segregate into three different polarimetric group according to distribution in Stokes plane. Solid lines in Figure 9 represent the changing direction of the vector P_V while connecting the weighted mean values of Q_V and U_V for the possible three different groups. The nearby group consists of ten member stars (namely, #5, #33, #35, #62, #63, #65a, #82, #95, #68M, #34M; Identification number suffix by "M" is according to ID(M) and others ac-

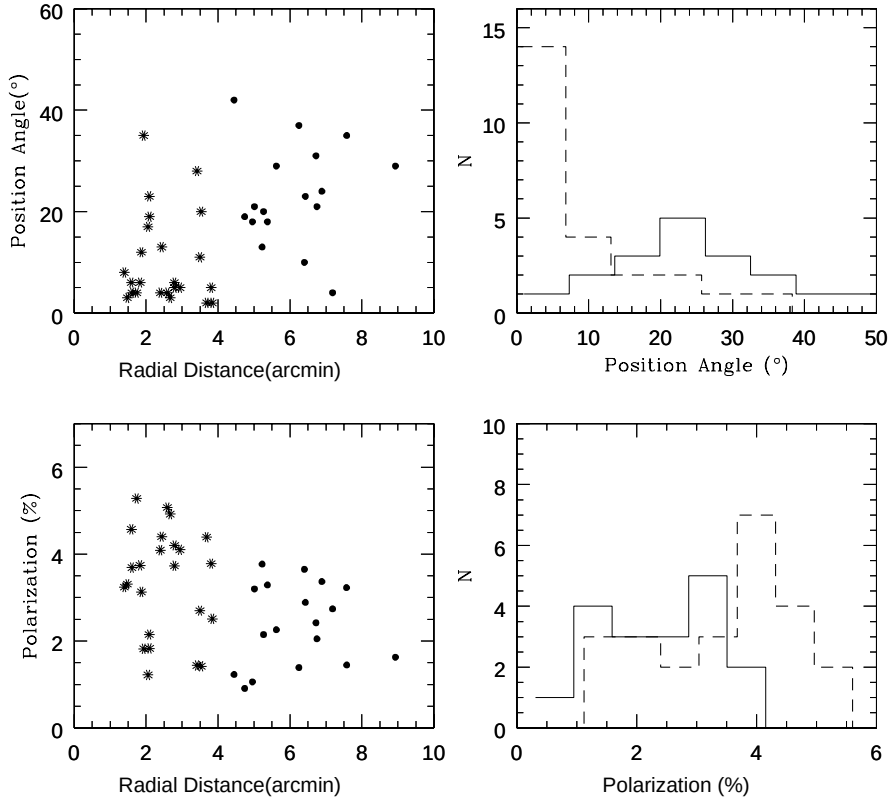

Figure 5. Distribution of P_V and PA_V for the 42 member stars with the radial distance from the cluster center

cording to ID(B)), with a weighted mean value of polarization $1.34 \pm 0.04\%$ and position angle $33 \pm 1^{\circ}$. This nearby group lies almost parallel to the Galactic Plane. The next group has six member stars (namely, #8, #36, #75, #80, #179, #58M) with weighted mean value of polarization and position angle $1.93 \pm .05\%$ and $23 \pm 1^{\circ}$, respectively. The remaining twenty six member stars (namely, #9, #11, #13, #14, #17, #20, #23, #25, #28, #34, #65, #68, #70, #74, #76, #78, #79, #91, #93, #185, #186, #187, #9M, #39M, #80M, #103M) are in the third group, which has a weighted mean value of polarization $3.64 \pm 0.01\%$ and position angle $11 \pm 1^{\circ}$.

The evolution of polarization towards NGC 6823 is likely to be due to patchy distribution of dust and the core may be behind a low dense layer of dust or a hole. Some of the authors who made the photometric studies of NGC 6823 believe that towards this cluster the distribution of dust is patchy, e. g. ; Guetter(1992) indicates that the reddening towards this cluster may be constant in small spatial areas but is highly variable across the face of the cluster and ranges from 1.07 to 0.64 mag. This absorption variability has been also noticed by many earlier investigators and can easily be seen by examining the color-magnitude and color-color plots as published by Hoag *et al.* (1961).

From the optical photometric study, Neckel and Klare (Neckel & Klare, 1980) found that more than half of the total extinction towards the cluster NGC 6823 comes from the matter lying close to us, at a distance between 0.2 to 0.5 kpc. The presence of a nearby interstellar matter at a distance of ~ 300 pc in the direction of cluster was also recently confirmed by Fresneau & Moiner (1999). They noticed a systematic absorption of about $1^m.5$ in V band in this region. The absorbing matter in this region may be probably located at a depth of the Vulpecula rift molecular cloud (Dame & Thaddeus, 1985). Therefore, we believe that the observed polarization towards NGC 6823 is mainly due to layers of nearby aligned dust grains of patchy structure associated with the above mentioned clouds.

3.2 Serkowski Law

The maximum wavelength (λ_{max}) and the maximum polarization (P_{max}) both are the functions of optical properties and characteristic of particle size distribution of the aligned dust grains (McMillan 1978, Wilking et al. 1980). Moreover, it is also related to the interstellar extinction law (Serkowski, Mathewson & Ford 1975, Whittet & van Breda 1978, Coyne & Magalhaes 1979, Clayton & Cardelli 1988). The λ_{max} and P_{max} have been calculated by fitting the observed polarization in the B, V and R_c band-passes to the standard Serkowski's polarization law;

$$P_\lambda / P_{max} = exp\left[- k\ ln^2\ (\lambda_{max}/\lambda)\right] \qquad (5)$$

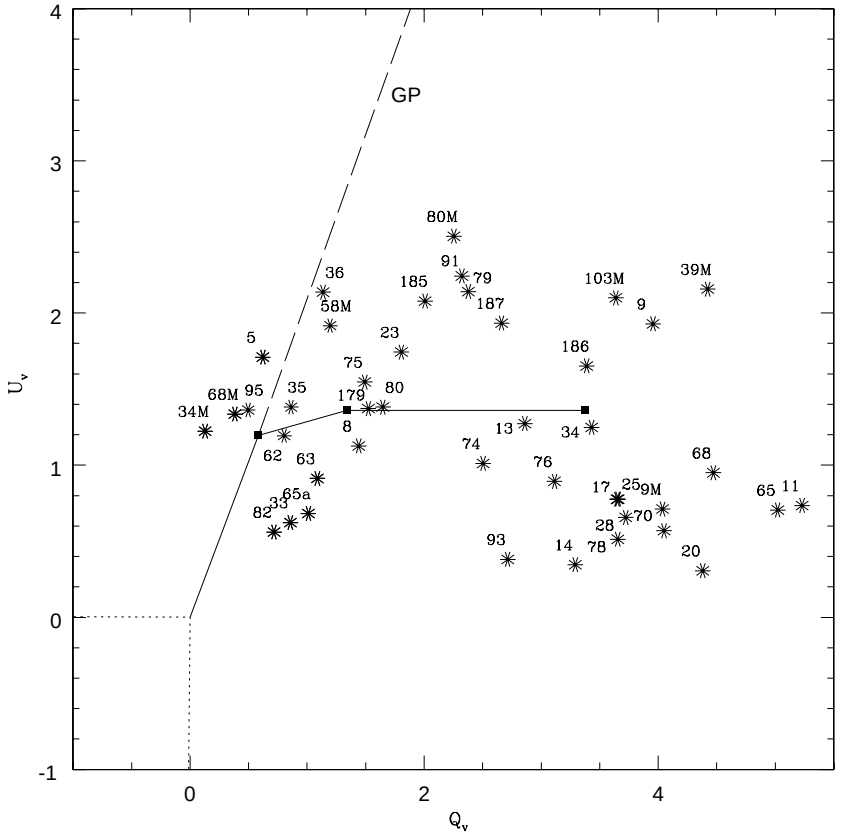

Figure 9. The U_V vs. Q_V plot for 42 member stars observed by us in the direction of NGC 6823. The dashed line is in the direction of the Galactic Plane (GP). The solid line is the interpretation of the evolution of polarization through the dust layer between the cluster and the Sun.

and adopting the parameter $k = 1.15$ (Serkowski 1973). In the fits the degree of freedom is adopted as one. Though there are only three data points, the wavelength covered ranges from 0.44 to 0.66 μm and all the λ_{max} found to fall within this range. Since, we have enough wavelength coverage, the fit is reasonably fine but sometimes it over estimates the value of σ_1. For each star we computed σ_1 parameter (the unit weight error of the fit). If the polarization is well represented by the Serkowski's interstellar polarization law, σ_1 should not be higher than 1.6 due to the weighting scheme. A higher value could be indicative of the presence of intrinsic polarization. The λ_{max} can also give us the clue about the origin of polarization. The stars which have λ_{max} lower than the average value of the interstellar medium (0.55±0.04 μm, Serkowski *et al.* 1975) are the probable candidates to have an intrinsic component of polarization (Orsatti, Vega & Marraco 1998). The dispersion of the position angle ($\overline{\epsilon}$) for each star normalized by the mean value of the position angle errors is the another tool to detect the intrinsic polarization. The values obtained for P_{max}, λ_{max}, σ_1 and $\overline{\epsilon}$ together with ID(M), ID(B), R.A.(2000J) and Dec(2000J) for all the 104 observed stars with their respective errors are given in Table 5 and 6. Column 9 in the Table 5 and 6 represent $E(B-V)$, available only for 21 member stars and 5 non-member stars. In that table the values of $E(B-V)$ sufix by (G), (S) and (E) taken from Guetter 1992, Stone 1988 and Erickson 1971 respectively.

Out of 104 stars observed by us, only for one non-member star (namely, #57M) and three member stars (namely, #08M, #40M and #102M) found the value of σ_1 above the limit of 1.6. The dispersion in the position angle $\overline{\epsilon}$ is found to be higher for one member star (namely, #25M) and eight non-member stars (namely, #15M, #21M, #45M, #70M, #78M, #87M, #88M and #101M). The λ_{max} for above mentioned thirteen stars detected by using two criteria σ_1 and $\overline{\epsilon}$ are nearly equal to the interstellar medium except the non-member star #78M. Although the non-member star #78M is found to have lower value of λ_{max} and higher value of $\overline{\epsilon}$ but the σ_1 is lower than the threshold. Therefore, the polarization towards NGC6823 is found to be mainly because of the foreground interstellar dust grains.

If the polarization is mainly dominated by the dust particles present in the diffuse interstellar medium the value of λ_{max} should be nearly equal to 0.55 ± 0.04 μm. The weighted mean of λ_{max} for the observed member and non-member stars of NGC 6823 are obtained as 0.53 ± 0.01 μm and 0.54±0.01 μm, respectively. The nearly similar values of λ_{max} for the member and the non-member stars imply that the lights from the both member and non-member stars encountering the same population of foreground dust grains.

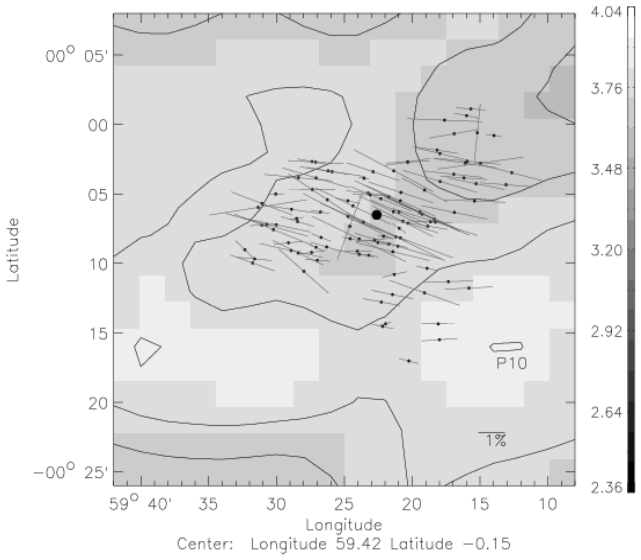

Figure 7. The high resolution extinction map of the region ($30' \times 30'$) produced by Dobashi et al. (2005) using the optical database 'Digitized Sky Survey I' and applying traditional star count technique. We overlay V band results from our observations using vectors drawn in black colours. The clump identified by Dobashi et al. (2005) in this region is identified and labeled as P10. The center of the cluster ($l = 59.40°$, $b = -0.14°$) is identified using black circle.

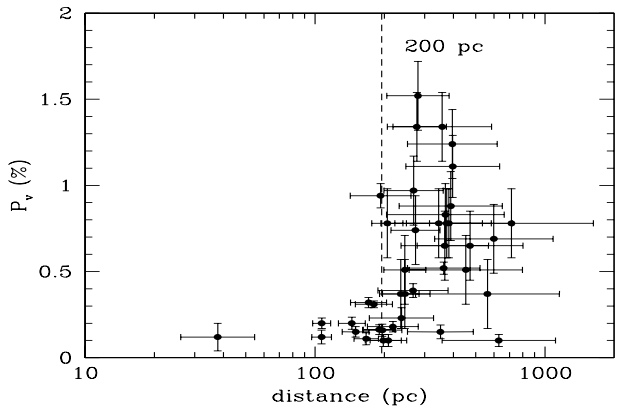

Figure 8. Distance versus $P_V\%$ plot, data obtained from Heiles (2000) and Perryman *et al.* (1997). The dotted line is drawn at 200 pc to show a sharp increase in $P_V\%$ value at these distance.

Therefore, the characteristic grain size distribution as indicated by the polarization study of stars in NGC 6823 is nearly same as that for the general interstellar medium. The weighted mean of the maximum polarization for the member and non-member stars are found as 2.82 ± 0.01 % and 1.76 ± 0.01 %, respectively.

3.3 Polarization efficiency

For interstellar dust particles in diffuse interstellar medium the ratio between the maximum amount of polarization to visual extinction (polarization efficiency) can not exceed the empirical upper limit (Hiltner 1956),

$$P_{max} < 3A_V \simeq 3R_V \times E(B-V) \quad (6)$$

The ratio $P_{max}/E(B-V)$ mainly depends on the alignment efficiency, magnetic strength and the amount of depolarization due to radiation traversing more than one cloud in different direction.

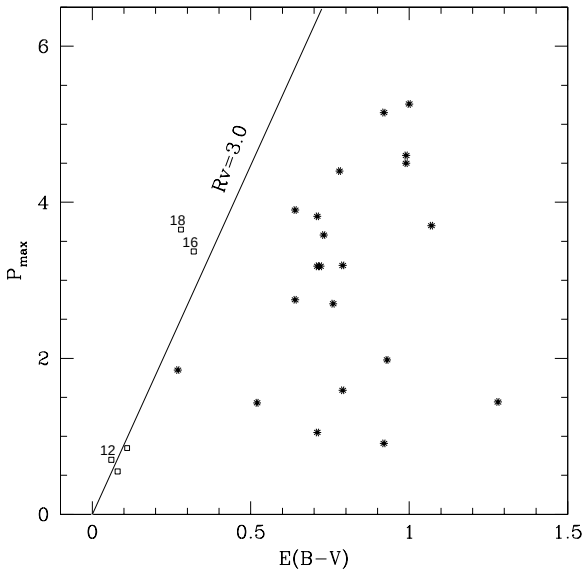

Figure 10. Polarization efficiency diagram. Using Rv=3.0, the line of maximum efficiency drawn. The stars observed by us in the direction of NGC 6823 are shown using open black square. The stars with $M_p \geqslant 0.50$ are identified using star symbol.

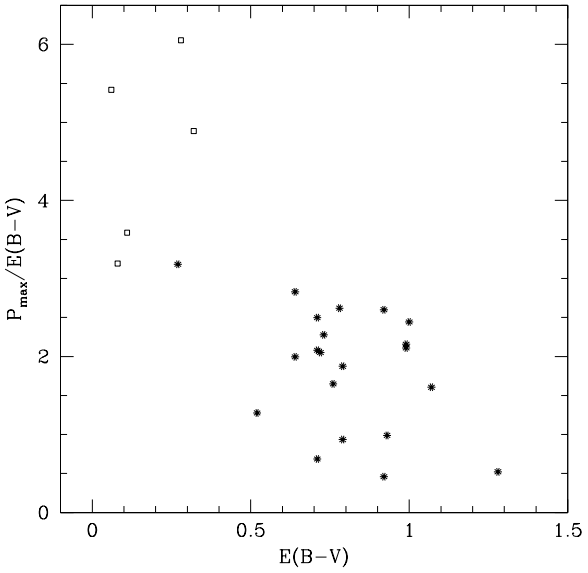

Figure 11. $P_{max}/E(B-V)$ plotted as a function of $E(B-V)$. The stars observed by us in the direction of NGC 6823 are shown using open black square. The stars with $M_p \geqslant 0.50$ are identified using star symbol.

Table 5. The P_{max}, λ_{max}, σ_1 & $\overline{\epsilon}$ for the observed data in NGC 6823.

ID(M)† (1)	ID(B)†† (2)	R.A(2000J) (3)	DEC(2000J) (4)	$P_{max}\pm\epsilon$ (%) (5)	$\lambda_{max}\pm\epsilon$ (μm) (6)	σ_1 (7)	$\overline{\epsilon}$ (8)	$E(B-V)$ (9)
01	—	19 42 51.00	23 18 42.2	2.08 ±0.11	0.50 ±0.05	0.36	0.48	—
02	20	19 42 54.82	23 18 59.6	4.40 ±0.01	0.56 ±0.01	0.18	0.44	0.78(G)
03	74	19 42 58.40	23 20 16.9	2.70 ±0.01	0.53 ±0.01	0.75	0.44	0.76(G)
04	73	19 43 01.60	23 20 37.7	0.53 ±0.01	0.55 ±0.01	0.10	0.21	—
05	18	19 42 59.58	23 17 45.9	3.65 ±0.08	0.55 ±0.03	0.59	0.81	0.28(G)
06	23	19 42 55.14	23 16 20.4	2.52 ±0.01	0.58 ±0.01	0.02	0.60	—
07	17	19 43 01.94	23 17 30.3	3.90 ±0.01	0.54 ±0.01	1.09	0.33	0.64(S)
08	78	19 43 02.76	23 18 22.8	3.58 ±0.14	0.60 ±0.04	2.68	0.44	0.73(G)
09	—	19 43 02.06	23 15 37.4	4.32 ±0.08	0.53 ±0.02	0.75	0.33	—
10	27	19 43 02.84	23 14 49.2	2.16 ±0.02	0.58 ±0.01	0.22	0.86	—
11	26	19 43 04.45	23 14 49.5	2.02 ±0.02	0.51 ±0.01	0.58	0.67	—
12	13	19 43 06.85	23 16 12.6	3.18 ±0.03	0.54 ±0.02	0.99	0.89	0.71(G)
13	28	19 43 01.53	23 14 40.8	3.83 ±0.01	0.60 ±0.01	0.02	0.53	—
14	75	19 43 05.01	23 19 50.0	2.25 ±0.04	0.56 ±0.03	0.65	0.19	—
15	77	19 43 05.17	23 19 37.9	1.72 ±0.01	0.54 ±0.01	0.03	1.20	—
16	76	19 43 04.49	23 18 49.4	3.28 ±0.02	0.56 ±0.01	0.69	0.67	—
17	16	19 43 06.03	23 17 33.1	3.37 ±0.20	0.55 ±0.07	1.33	0.29	0.32(G)
18	71	19 43 10.33	23 20 51.0	1.15 ±0.14	0.50 ±0.12	1.41	0.92	—
19	70	19 43 10.91	23 20 20.8	4.12 ±0.01	0.51 ±0.01	0.06	0.67	—
20	68	19 43 13.62	23 19 05.8	4.60 ±0.02	0.51 ±0.01	1.11	0.44	0.99(G)
21	12	19 43 09.60	23 16 35.3	0.70 ±0.06	0.60 ±0.08	0.69	1.13	0.06(G)
22	11	19 43 12.46	23 16 29.8	5.26 ±0.03	0.52 ±0.01	0.87	0.33	1.00(G)
23	4	19 43 14.28	23 17 18.5	0.55 ±0.01	0.54 ±0.01	0.01	0.05	0.08(G)
24	9	19 43 14.69	23 16 01.5	4.50 ±0.04	0.49 ±0.02	1.57	0.22	0.99(G)
25	8	19 43 15.52	23 16 41.0	1.85 ±0.02	0.56 ±0.03	0.48	1.62	0.27(G)
26	5	19 43 16.67	23 17 44.7	1.67 ±0.15	0.52 ±0.14	1.42	1.18	—
27	64a	19 43 16.98	23 19 48.7	3.44 ±0.02	0.52 ±0.01	0.15	0.50	—
28	65	19 43 18.91	23 18 45.6	5.15 ±0.11	0.54 ±0.03	0.84	0.76	0.92(G)
29	64	19 43 20.30	23 19 20.6	0.85 ±0.02	0.52 ±0.03	0.24	0.18	0.11(G)
30	62	19 43 22.55	23 18 26.6	1.44 ±0.01	0.56 ±0.01	0.02	0.25	1.28(E)
31	61	19 43 21.83	23 17 33.6	0.97 ±0.01	0.51 ±0.02	0.16	0.44	—
32	63	19 43 23.11	23 18 11.6	1.46 ±0.03	0.54 ±0.03	0.23	0.41	—
33	65a	19 43 16.90	23 17 26.6	1.28 ±0.03	0.57 ±0.04	0.22	0.06	—
34	—	19 43 22.96	23 15 14.7	1.07 ±0.09	0.56 ±0.13	0.88	0.52	—
35	25	19 43 02.04	23 15 49.5	3.82 ±0.14	0.57 ±0.08	1.43	0.36	0.71(G)
36	—	19 43 05.18	23 17 10.7	3.08 ±0.01	0.50 ±0.01	0.06	0.52	—
37	10	19 43 12.04	23 16 10.1	6.05 ±0.07	0.50 ±0.01	0.53	0.40	—
38	—	19 43 16.98	23 16 09.5	3.61 ±0.02	0.52 ±0.01	0.16	0.74	—
39	—	19 43 14.54	23 20 17.0	5.07 ±0.05	0.53 ±0.01	1.03	0.56	—
40	14	19 43 07.13	23 16 35.8	3.18 ±0.12	0.55 ±0.06	3.59	0.22	0.72(G)
41	33	19 43 16.05	23 13 22.0	1.05 ±0.01	0.55 ±0.01	0.05	0.36	0.71(S)
42	36	19 43 16.27	23 11 31.7	2.42 ±0.01	0.56 ±0.01	0.01	0.74	—
43	—	19 43 14.72	23 09 59.2	2.37 ±0.02	0.53 ±0.01	0.07	0.27	—
44	34	19 43 23.11	23 12 39.5	3.70 ±0.01	0.54 ±0.01	0.33	0.22	1.07(G)
45	51	19 43 28.70	23 14 38.5	2.07 ±0.03	0.55 ±0.03	0.40	1.00	—
46	53	19 43 32.51	23 15 04.9	1.86 ±0.01	0.53 ±0.01	0.02	0.36	—
47	35	19 43 29.37	23 10 39.7	1.59 ±0.02	0.53 ±0.02	0.62	0.22	0.79(S)
48	50	19 43 37.73	23 14 02.4	0.59 ±0.01	0.57 ±0.01	0.30	0.37	—
49	49	19 43 38.93	23 14 07.1	1.12 ±0.04	0.50 ±0.07	0.82	0.87	—
50	—	19 43 33.47	23 10 01.2	1.80 ±0.01	0.58 ±0.02	0.10	0.59	—
51	42	19 43 44.14	23 11 12.7	0.98 ±0.01	0.56 ±0.01	0.23	0.26	—
52	98	19 43 05.38	23 24 32.8	1.47 ±0.02	0.59 ±0.02	0.11	0.16	—
53	99	19 43 04.96	23 24 17.6	2.69 ±0.10	0.50 ±0.03	0.39	0.36	—
54	80	19 43 05.36	23 23 11.1	1.90 ±0.08	0.57 ±0.05	1.04	0.33	—
55	79	19 43 04.93	23 22 54.4	3.21 ±0.01	0.55 ±0.01	0.02	0.57	—
56	—	19 43 09.17	23 23 42.1	3.37 ±0.01	0.55 ±0.01	0.04	0.37	—
57	81	19 43 13.32	23 22 12.2	4.41 ±0.22	0.51 ±0.07	2.22	0.74	—
58	—	19 43 12.91	23 23 32.2	2.15 ±0.08	0.54 ±0.06	0.50	0.35	—
59	82	19 43 17.75	23 22 12.3	0.91 ±0.01	0.52 ±0.01	0.09	0.09	0.92(S)
60	125	19 43 20.03	23 25 42.1	0.71 ±0.04	0.55 ±0.10	1.16	0.21	—
61	—	19 43 21.66	23 24 08.7	2.77 ±0.14	0.60 ±0.08	0.98	0.35	—
62	—	19 43 23.35	23 23 29.7	0.66 ±0.01	0.59 ±0.03	0.31	0.33	—

Table 6. Continuation of Table 5

ID(M)† (1)	ID(B)†† (2)	R.A(2000J) (3)	DEC(2000J) (4)	$P_{max}\pm\epsilon$ (%) (5)	$\lambda_{max}\pm\epsilon$ (μm) (6)	σ_1 (7)	$\overline{\epsilon}$ (8)	$E(B-V)$ (9)
63	96	19 43 24.02	23 23 19.2	1.74 ±0.04	0.51 ±0.03	0.20	0.33	—
64	—	19 43 24.83	23 26 14.7	3.01 ±0.12	0.51 ±0.04	0.50	0.24	—
65	—	19 43 26.47	23 26 21.1	4.97 ±0.07	0.53 ±0.02	0.36	0.53	—
66	—	19 43 26.27	23 20 33.3	1.65 ±0.02	0.51 ±0.02	0.14	0.40	—
67	88	19 43 28.09	23 21 13.0	0.71 ±0.01	0.52 ±0.04	0.46	0.15	—
68	—	19 43 30.17	23 21 19.4	1.39 ±0.01	0.50 ±0.01	0.10	0.17	—
69	86	19 43 31.42	23 20 40.3	1.11 ±0.11	0.51 ±0.11	0.76	0.11	—
70	127	19 43 28.34	23 24 34.1	3.38 ±0.02	0.58 ±0.01	1.10	1.67	—
71	130	19 43 30.70	23 25 29.0	1.23 ±0.01	0.59 ±0.03	0.20	0.58	—
72	129	19 43 29.84	23 25 10.7	4.09 ±0.07	0.50 ±0.02	0.44	0.56	—
73	95	19 43 31.27	23 23 08.5	1.43 ±0.01	0.55 ±0.02	0.36	0.57	0.52(G)
74	93	19 43 32.43	23 22 09.7	2.75 ±0.01	0.50 ±0.01	0.31	0.67	0.64(G)
75	94	19 43 32.95	23 22 41.6	3.01 ±0.13	0.51 ±0.04	0.43	0.83	—
76	91	19 43 36.55	23 21 08.5	3.19 ±0.02	0.55 ±0.01	0.48	0.56	0.79(S)
77	—	19 43 40.13	23 25 41.3	1.29 ±0.01	0.49 ±0.01	0.14	0.60	—
78	—	19 43 41.07	23 24 44.0	1.59 ±0.08	0.49 ±0.04	0.48	1.17	—
79	—	19 43 42.50	23 24 42.7	2.21 ±0.14	0.59 ±0.07	0.66	0.48	—
80	—	19 43 11.95	23 24 50.7	3.49 ±0.06	0.57 ±0.02	0.32	0.72	—
81	128	19 43 30.09	23 24 34.4	4.25 ±0.06	0.56 ±0.02	0.52	0.24	—
82	—	19 43 24.58	23 21 15.3	0.95 ±0.05	0.51 ±0.07	0.40	0.42	—
83	—	19 42 25.70	23 16 16.3	1.41 ±0.11	0.53 ±0.12	1.41	0.83	—
84	—	19 42 28.22	23 16 18.4	1.19 ±0.01	0.50 ±0.02	0.26	0.67	—
85	—	19 42 29.26	23 13 50.4	0.77 ±0.01	0.55 ±0.02	0.66	0.75	—
86	—	19 42 31.16	23 15 00.4	2.83 ±0.03	0.57 ±0.02	0.09	0.26	—
87	—	19 42 32.97	23 17 33.5	3.69 ±0.01	0.52 ±0.01	0.16	1.33	—
88	—	19 42 35.12	23 16 27.4	2.46 ±0.01	0.53 ±0.01	0.02	1.25	—
89	—	19 42 36.55	23 11 22.3	3.38 ±0.03	0.57 ±0.02	0.16	0.33	—
90	—	19 42 38.92	23 13 43.4	4.34 ±0.07	0.57 ±0.03	0.40	0.93	—
91	—	19 42 40.51	23 14 38.1	3.26 ±0.02	0.52 ±0.02	0.25	0.47	—
92	184	19 42 41.38	23 14 41.3	3.29 ±0.07	0.51 ±0.03	0.67	0.67	—
93	179	19 42 42.33	23 16 57.6	1.98 ±0.05	0.53 ±0.03	0.51	0.57	0.93(E)
94	180	19 42 42.79	23 16 39.5	2.57 ±0.01	0.52 ±0.01	1.10	0.22	—
95	—	19 42 40.72	23 11 18.6	2.57 ±0.05	0.50 ±0.02	0.24	0.61	—
96	191	19 42 45.20	23 13 15.9	2.68 ±0.08	0.53 ±0.04	0.51	0.33	—
97	—	19 42 45.58	23 14 15.0	2.28 ±0.01	0.57 ±0.03	0.16	0.76	—
98	185	19 42 46.19	23 15 02.0	2.88 ±0.01	0.52 ±0.01	0.08	0.74	—
99	22	19 42 50.25	23 18 25.4	2.28 ±0.01	0.52 ±0.01	0.03	0.13	—
100	186	19 42 50.32	23 15 39.1	3.77 ±0.01	0.55 ±0.01	0.32	0.67	—
101	192	19 42 50.17	23 12 45.2	2.81 ±0.07	0.51 ±0.04	0.72	1.83	—
102	187	19 42 56.48	23 13 37.9	3.26 ±0.09	0.55 ±0.08	4.66	0.44	—
103	—	19 43 02.16	23 16 14.1	4.22 ±0.01	0.51 ±0.01	0.02	0.21	—
104	29	19 43 02.13	23 14 30.4	4.39 ±0.05	0.50 ±0.02	1.28	0.33	—

† : According to this observation
†† : According to Barkhatova (1957)
(G) : According to Guetter (1992)
(S) : According to Stone (1988)
(E) : According to Erickson (1971)

Figure 10 shows the relation between colour excess $E(B-V)$ and maximum polarization P_{max} for the stars observed by us (open square symbol for non-member and star symbol for member stars) towards NGC 6823 produced by the dust grains along the line of sight to the cluster. Out of the 104 stars observed by us $E(B-V)$ is available only for 26 stars (21 member and 5 non-member stars). In the polarization efficiency diagram three non-member stars #12, #16 and #18 (identification according to ID(B)) are lying to the left side of the interstellar maximum line, which imply that these three stars may be affected by intrinsic polarization. In case of star #12 the dispersion in the position angle $\overline{\epsilon}$ is found to be higher (1.13) but the σ_1 is lower than the threshold. Apparently, the dominant mechanism of polarization for the observed member stars of NGC 6823 is supposed to be the selective absorption by the interstellar dust grains which are aligned by the local and galactic magnetic field. Also the Figure 10 indicates that while the colour excess for the member stars of NGC 6823 varies from 0.27 to 1.28 mag approximately, the variation in the polarization value is very high $\sim$ 4.5%. High variation of P_{max} indicates the different

populations of dust grains may be present in the line of sight towards NGC 6823, as inferred from the Section 3.1.

In Figure 11, we plot the $P_{max}/E(B-V)$ vs. $E(B-V)$ for the 104 stars observed by us with available colour excess $E(B-V)$(black open square symbol for non-member and star symbol for member stars). The polarization efficiency is found to fall with the increase in $E(B-V)$. The decrement of polarization efficiency with increase in $E(B-V)$ may be because of increase in the size of the dust grains or small change in the polarization position angle.

4 SUMMARY

The main results of this study are summarized as follows:

We have observed the linear polarization for 104 stars in the region of open cluster NGC 6823. The analysis of these data show that the polarization is mostly due to the foreground dust grains distributed in patchy pattern and the majority of the observed stars do not present the indication of intrinsic polarization. We also found the evidence of several dust layers/components along the line of sight to the cluster. Combining our results with those from the literature, we present the evidence for the presence of first layer of dust located approximately within 200 pc towards the cluster.

The radial distribution of the position angles for the member stars are found to show a systematic change while the polarization found to reduce towards the outer parts of the cluster. The average position angle of the member stars belongs to the coronal region is more closer to the inclination of the Galactic parallel ($\sim 32^{\circ}$) than the nuclear region of the cluster.

Polarization efficiency for the cluster member stars are nearly similar to that for the field stars, which imply that the similar polarization mechanism is responsible for both the member and the field stars towards the cluster.

The weighted mean of maximum wavelength λ_{max} for the cluster members and the field stars are found to be 0.53 ± 0.01 μm and 0.54 ± 0.01 μm, respectively. These values of λ_{max} of stars towards NGC 6823 are thus similar to those of interstellar medium (0.55 ± 0.04 μm). Therefore the polarization towards NGC 6823 is caused mainly due to the foreground dust grains as we have inferred for the clusters IC 1805 and NGC 654 (Medhi *et al.* 2007, 2008). The intracluster dust grains are very similar to that of the general interstellar medium.

ACKNOWLEDGMENTS

The authors thank the referee Prof. Carlos Feinstein for his constructive comments and suggestions which have lead to substantial improvements of the paper. It is also our pleasure thank Prof. H. C. Bhatt for his useful suggestions. This research has made use of the WEBDA database, operated at the Institute for Astronomy of the University of Vienna, use of image from the National Science Foundation and Digital Sky Survey (DSS), which was produced at the Space Telescope Science Institute under the US Government grant NAG W-2166; use of NASA's Astrophysics Data System and use of IRAF, distributed by National Optical Astronomy Observatories, USA. The author (BJM) like to thank his daughter Sanskriti and wife Orchid for their support.

REFERENCES

Barkhatova K.A. 1957, Soviet Astron. J. 1, 827
Chapin, E. L., Ade, P. A. R., Bock, J. J., Brunt, C., Devlin, M. J., Dicker, S. *et al.* , 2008, ApJ, 681, 428
Clayton, G. C., Cardelli, J. A., 1988, AJ, 96, 695
Corradi, Romano L. M., Aznar, R., Mampaso, A., 1998, MNRAS, 297, 617
Coyne, G. V., Magalhaes, A. M., 1979, AJ, 84, 1200
Dame, T. M.; Thaddeus, P.; 1985, Astrophys.J.,170 325.
Davis, Leverett, Jr.; Greenstein, Jesse L.; 1951, ApJ, 114, 206
Dias, W. S., Assafin, M., Flrio, V., Alessi, B. S., Lbero, V.,2006, A&A, 446, 949
Dobashi, K., Uehara, H., Kandori, R., Sakurai, T., Kaiden, M., Umemoto, T., Sato, F., 2005, PASJ, 57, 1
Erickson R.R., 1971, A&A,10, 270
Feinstein, A., 1994, RMxAA, 29, 141
Fresneau, A.; Monier, R.; 1999, AJ,118,421.
Goldreich, Peter, Kwan, John, 1974, ApJ, 189, 441
Guarinos J., 1992, Astronomy from Large Databases II", ESO Conference and Workshop Proceedings No 43, ISBN 3-923524-47-1, 301
Guetter, H. H.; 1992, AJ 103, 197.
Guetter, Harry H., Vrba, Frederick J., 1989, AJ, 98, 611
Hall, John Scoville, 1958, PUSNO, 17, 1
Heiles, Carl; 2000, AJ, 119, 923
Hiltner, W. A., 1956, ApJS, 2, 389
Hoag, A. A., Johnson, H. L., Iriarte, B., Mitchell, R. I., Hallam, K. L., Sharpless, S.; 1961, PUSNO, 17, 343
Hϕg, E., Bässgen, G., Bastian, U., Egret, D., Fabricius, C., Groβmann, V. *et al.* , 1997, A&A, 323, 57
Jones, R. Victor, Spitzer, Lyman, Jr., 1967, ApJ, 147, 943
Kharchenko N.V., Piskunov A.E., Rser S., Schilbach E., Scholz R.D., 2005, A&A, 438, 1163
Lazarian, A., Goodman, Alyssa A., Myers, Philip C., 1997, ApJ, 490, 273
Leisawitz, David, Bash, Frank N., Thaddeus, Patrick, 1989, ApJS, 70, 731
Lynds, Beverly T., 1962, ApJS, 7, 1
McMillan, R. S., 1978, APJ, 225, 880
Medhi, Biman J., Maheswar, G., Brijesh, K., Pandey, J. C., Kumar, T. S., Sagar, R.,2007, MNRAS, 378, 881
Medhi, Biman J., Maheswar, Pandey, J. C., Kumar, T. S., Sagar, R.,2008, MNRAS, 388, 105
Morgan, W. W., Whitford, A. E. and Code, A. D.; 1953, Astrophys.J.118,318.
Neckel, Th., Klare, G., 1980, A&ASS, 42 251.
Orsatti, A. M., Vega, E., Marraco, H. G., 1998, AJ, 116, 266
Pandey, J. C., Medhi, Biman J., Sagar, R., Pandey, A. K., 2009, MNRAS, 396, 1004
Perryman, M. A. C., Lindegren, L., Kovalevsky, J., Hϕg, E., Bastian, U., Bernacca, P. L. *et al.* , 1997, A&A, 323, 49
Ramaprakash, A. N., Gupta, R., Sen, A. K., Tandon, S. N., 1998, A&AS, 128, 369
Rautela, B. S., Joshi, G. C., Pandey, J. C., 2004, BASI, 32,159

Sagar, R. and Joshi, U. C.; 1981, Ap&SS 75, 465.
Sagar, R., Joshi, U. C., Sinvhal, S. D., 1983, BASI, 11, 44
Sagar, R.; 1987, MNRAS, 228, 483
Serkowski, K., 1965, ApJ, 141, 1340
Serkowski, K., 1973, IAUS, 52, 145
Serkowski, K.; Mathewson, D. L.; Ford, V. L.; 1975, ApJ, 196, 261
Schmidt, G. D., Elston, R., Lupie, O. L., 1992, AJ, 104, 1563
Spitzer, Lyman, 1978, Physical processes in the interstellar medium, John Willy & sons, New York
Stone, Ronald C.,1988, AJ, 96, 1389
Turner, D. G., 1979, JRASC, 73, 74
Turnshek, D. A., Bohlin, R. C., Williamson, R. L., II, Lupie, O. L., Koornneef, J., Morgan, D. H., 1990, AJ, 99, 1243
Wilking, B. A., Lebofsky, M. J., Kemp, J. C., Martin, P. G., Rieke, G. H., 1980, ApJ, 235, 905
Whittet, D.C.B., van Breda, I.G., 1978, A&A, 66, 57
Whittet, D. C. B., 1992, Dust in the Galactic Environment (Bristol:IOP)

This paper has been typeset from a TEX/ LATEX file prepared by the author.

Mon. Not. R. Astron. Soc. **000**, 1 (2001) Printed 21 December 2009 (MN LaTeX style file v2.2)

New features in the *Monthly Notices* LaTeX 2$_\varepsilon$ class file

2001 February 06

The MNRAS LaTeX 2$_\varepsilon$ class file is implemented by placing the command
`\documentclass[`*options*`]{mn2e}`
at the start of the document.

The various `option` commands listed in the *Monthly Notices* LaTeX style guide for authors can still be used. The following additional options exist.

(i) `useAMS` – this enables the production of upright Greek characters π, μ and ∂ (`$\upi$`, `$\umu$` and `$\upartial$`) and slanted $\leqslant$ and $\geqslant$ (`$\leq$` and `$\geq$`). Characters π, μ and ∂ appear upright only on systems that have the Euler roman fonts (`eurm`*xx*); characters $\leqslant$ and $\geqslant$ appear slanted only on systems that have the AMS series A fonts (`msam`*xx*). On systems that do not have these fonts, the standard forms of the characters appear in the printout; however, they should be correct in the final typeset paper if the correct LaTeX commands have been used.

(ii) `usedcolumn` – this uses the package file `dcolumn.sty` to define two new types of column alignment for use in tables. If the `usedcolumn` option has been specified then, within a table, `d{`*x*`}` can be used to produce a 'flush right' decimal-aligned column with *x* decimal places and `.` can be used to provide a decimal-aligned column centred on the decimal point (the number of decimal places does not need to be specified for this column type). Note that the standard LaTeX 'tools' packages `dcolumn.sty` and `array.sty` are required in order to use the `usedcolumn` option.

(iii) `usenatbib` – this uses Patrick Daly's `natbib.sty` package for cross-referencing. If the `usenatbib` option is specified, citations in the text should be in one of the following forms (or one of the additional forms documented within `natbib.sty` itself).

- `\citet{`*key*`}` produces text citations, e.g. Jones et al. (1990),
- `\citep{`*key*`}` produces citations in parentheses, e.g. (Jones et al. 1990),
- `\citealt{`*key*`}` produces citations with no parentheses, e.g. Jones et al. 1990.

For three-author papers, a full author list can be forced by putting a `*` just before the `{`. To add notes within the citation, use the form `\citep[`*pre_reference_text*`][`*post_reference_text*`]{`*key*`}` (note that either of *pre_reference_text* and *post_reference_text* can be blank).

Items in the reference list must be of the form
`\bibitem[\protect\citeauthoryear{`*author_names*`}{`*year*`}]{`*key*`}` Text of reference ...
for one-, two- and multi-author papers, or
`\bibitem[\protect\citeauthoryear{`*three_author_names*`}{`*first_author_etal*`}{`*year*`}]{`*key*`}` Text of reference ...
for three-author papers.

Note that Patrick Daly's package `natbib.sty` is required in order to use the `usenatbib` option.

We recommend that authors use `natbib.sty` as their standard cross-referencing package, because of the flexibility in citation style that it provides.

(iv) `usegraphicx` – this loads the graphics package `graphicx.sty`, which authors can use to include figures in their papers. Note that the standard LaTeX graphics package `graphicx.sty` is required in order to use the `usegraphicx` option.

Other style files, or packages providing features such as graphics support, can be used in conjunction with `mn.cls`. To do this, the command `\usepackage{`*package_name*`}` is used.

An additional feature of the class file is that footnote symbols are now in the correct journal style (symbols for title page footnotes, superscript arabic numbers for text footnotes).

A BibTeX style file, `mn2e.bst`, is now available for authors who wish to use BiBTeX. It is recommended that this should be used in conjunction with `natbib.sty`.

For general instructions on preparing *Monthly Notices* papers in LaTeX, please refer to the MNRAS LaTeXstyle guide for authors, available on the CTAN sites in subdirectory `/tex-archive/macros/latex209/mnras`.